

Noise-induced escape in an excitable systemI. A. Khovanov,^{1,*} A. V. Polovinkin,² D. G. Luchinsky,^{3,4} and P. V. E. McClintock³¹*School of Engineering, University of Warwick, Coventry CV4 7AL, United Kingdom*²*Radiophysical Department, Nizhny Novgorod St. University, Gagarin Avenue, 23, Nizhny Novgorod, 603600, Russian Federation*³*Department of Physics, Lancaster University, Lancaster LA1 4YB, United Kingdom*⁴*Mission Critical Technologies Inc., 2041 Rosecrans Ave., Suite 225, El Segundo, California 90245, USA*

(Received 16 December 2012; published 7 March 2013)

We consider the stochastic dynamics of escape in an excitable system, the FitzHugh-Nagumo (FHN) neuronal model, for different classes of excitability. We discuss, first, the threshold structure of the FHN model as an example of a system without a saddle state. We then develop a nonlinear (nonlocal) stability approach based on the theory of large fluctuations, including a finite-noise correction, to describe noise-induced escape in the excitable regime. We show that the threshold structure is revealed via patterns of most probable (optimal) fluctuational paths. The approach allows us to estimate the escape rate and the exit location distribution. We compare the responses of a monostable resonator and monostable integrator to stochastic input signals and to a mixture of periodic and stochastic stimuli. Unlike the commonly used local analysis of the stable state, our nonlocal approach based on optimal paths yields results that are in good agreement with direct numerical simulations of the Langevin equation.

DOI: [10.1103/PhysRevE.87.032116](https://doi.org/10.1103/PhysRevE.87.032116)

PACS number(s): 05.40.-a, 05.45.-a, 87.10.-e, 84.35.+i

I. INTRODUCTION

Stochastic excitable dynamics of the type exhibited by the FitzHugh-Nagumo (FHN) model underlies many systems in biology, especially in neuroscience [1,2]. Nonbiological systems, e.g., lasers and semiconductors [3–7], also display excitable behavior, and it has come to be appreciated that excitable systems can usefully be considered as forming a distinct class characterized by their own particular modes of behavior.

The key feature of excitability observed experimentally is that the system under study exhibits qualitatively different responses to two stimuli that differ only slightly in magnitude: For example, a neuron may produce either spikes of large amplitude or small oscillations about an equilibrium; the shape of a spike does not depend on the stimulus. This leads to the widely accepted concept of a threshold, even though, in many cases, there is no saddle state forming the threshold. However, the detailed definition of excitability, even for neurons, remains vague. The reason is arguably the difficulty of providing a simplified model that accommodates, simultaneously, a diversity of neuronal structures and types of stimuli and responses. For example, neuroscience textbooks present the neuron as an integrator with a very well defined threshold, whereas Izhikevich [8] provides a definition based on dynamical systems theory in the form “neurons are excitable because they are near a transition, called a bifurcation, from resting to sustained spiking activity”; he stresses that, in general, there is no very well defined threshold. If we were to try to define excitability in terms of the neural response to a stochastic stimulus, then there would be yet another definition. Note that *multistable* systems are often called *excitable* on the basis that the system can be “excited” to perform a transition between states. In contrast, we distinguish between multistability and excitability by pointing out that the latter implies the recurrence

of an initial state after noise-induced motion, whereas the former assumes a transition from an initial state to another state. For topological reasons [9], a minimal system dimension of 2 is needed for such recurrence.

The choice of definition is not the end of the story, however, because excitability itself can also be classified, and in a manner that is important for neuroscience. Hodgkin’s classification [10] was based on experimental observations of how a neuron reacts to an increase of the *constant* current bias. Later, this classification was connected to the bifurcations that can occur in two-dimensional neuronal models [11]. Note that there is some confusion in the bifurcational classifications of excitability and that the issue has been extensively discussed by Izhikevich [8]. He suggested a new classification based on the dynamic description of two-dimensional neuronal models. He considers four types of excitable behavior related to different bifurcations of an equilibrium state involving a transition from the resting (fixed point) to periodic spiking (limit cycle) behavior of neurons. His bifurcational (local) classification uses two independent criteria (which is what leads to four classes): (i) the number of steady sets (fixed points and cycles) and (ii) the character of the stability (node or focus) of the stable state (fixed point). Therefore, a two-dimensional neuron model can be either an integrator (node) or a resonator (focus), with either bistable (fixed points or cycles) or monostable activity [8]. We adopt this classification in what follows below but relax the close connection with bifurcations.

We point out that, although Izhikevich provides [8] a comprehensive discussion and justification of such a classification, the main object of discussion was a deterministic neuron model and nearly all the supportive experimental results were based on a constant applied bias. In reality, however, a typical neuron receives stochastic and/or time-variable stimuli and, therefore, requires the use of a stochastic model. Due to the noise, the nonoscillatory neuron with a stable state changes into a system exhibiting both oscillatory and excitatory properties [12]. In the latter case, the question of a threshold is much more important than in the deterministic one because its structure

*i.khovanov@warwick.ac.uk

defines an activation process from a steady state to an excitable one, i.e., to a state capable of producing a spike.

Currently, approaches to the analysis of noise-induced escape in excitable systems are based on a fast-slow decomposition [1,13,14]. It leads to a one-dimensional (potential) problem where the threshold is introduced explicitly either as a saddle state or as a particular value of a coordinate. In the latter case, the fold point of the nullcline is often used [13]. In other words, the threshold is created artificially without any direct reference to the actual threshold structure of the initial system. Additionally, the decomposition assumes a small parameter (since it is based on an asymptotic deterministic description of excitability) so it is not applicable in all cases, e.g., the resonator case. Thus, the decomposition approach involves strong limitations in terms of system parameters, whereas the role of the threshold structure during noise-induced escape remains unclear.

Another problem of the fast-slow decomposition approach lies in the fact that the simultaneous consideration of noise sources in both the fast and slow variables is inherently difficult [13]. In neuroscience, noise in the fast variable of the neuron is typically considered as corresponding to the synaptic inputs arriving from other neurons. Noise in the slow variable is taken to arise from the intracellular intrinsic dynamics, e.g., the fluctuations of currents in ion channels. The latter noise has attracted less attention, even though it appears explicitly in the archetypical Hodgkin-Huxley model [15,16] and there is evidence that it plays an important role in neural regulatory networks [17]. Note that, in excitable lasers [5,7], noise is present in both the fast and slow variables.

In this paper, we overcome the limitations of the decomposition approach and discuss the stochastic dynamics of an excitable system for particular classes of excitability. We develop a nonlinear (nonlocal) approach to describe noise-induced escape and the role of the threshold structure in escape processes. The approach is based on the theory of large fluctuations [18]. It involves no limitations in terms of system parameters, but it assumes the small noise limit. Nonetheless, as we show below, it is actually applicable over a wide range of noise intensities. A condition of applicability is that the noise-induced excitation has an activation character, that is, the activation time must be longer than the time of relaxation to equilibrium. The approach developed is also applicable to the case when noises are acting in both the slow and fast variables. It takes account of finite noise intensity and allows us to calculate the exit location distribution analytically. We compare the predictions of the deterministic (local) approach [8] with the nonlocal approach that we develop. We do so by analyzing the responses of a monostable resonator and a monostable integrator to stochastic input signals and to a mixture of periodic and stochastic stimuli. We consider specifically the FHN neuron model, but we expect that the results can readily be extended for application to other models.

In Sec. II we discuss the excitability property and provide some heuristic comments on the existence of a threshold in the monostable case. Then, in Sec. III, we demonstrate the existence of a threshold via theoretical calculations of the most probable (optimal) escape path. Noise sources in both the slow and fast variables are considered. We also test the

theoretical conclusions against direct numerical simulations of the Langevin equation and discuss the threshold structure and its role in the noise activation process. In Sec. IV we compare activation paths for an integrator and a resonator by analysis of the optimal activation (escape) path and optimal fluctuational force, and we consider the effect of weak periodic driving on noise-induced spike generation for both the integrator and the resonator cases. Our main conclusions are summarized in Sec. V.

II. THE “GHOST” SEPARATRIX

In the present case we define an excitable system as one that is able to produce a spike in response to an external stimulus. The spike properties depend only insignificantly on the external stimulus, and the spikes are only observed for some nonzero stimulus amplitude, i.e., the external stimulus must exceed a threshold in order to excite a spike.

Note that, although the above definition is not universal, it describes well the excitable property of many systems, including that of the FHN system,

$$\begin{aligned}\dot{u} &= F(u,v) = u - \frac{u^3}{3} - v, \\ \dot{v} &= \epsilon G(u,v) = \epsilon[u + a].\end{aligned}\quad (1)$$

Here $u(t)$ and $v(t)$ represent the fast and slow variables, which may correspond, e.g., to the membrane potential and slow recovery of a neuron, respectively. The parameter ϵ describes the difference in time scales between the fast and slow variables, and the parameter a defines the regimes (bifurcations) of system (1).

We now consider the dynamics of (1) for the fixed values $a = 1.05$ and $\epsilon = 0.05$. The two curves given in Fig. 1, $F(u,v) = 0$ and $G(u,v) = 0$ [$G(u) = 0$ here], are nullclines i.e., boundaries between regions where the derivatives \dot{u} and \dot{v} are of opposite sign. The point of intersection of the nullclines is determined by the parameter a and corresponds to a fixed point of system (1). The nullcline $F(u,v) = 0$ forms a nonmonotonic curve that can be divided into three branches: The right $F_r(u,v)$ and left $F_l(u,v)$ branches and the middle branch $F_m(u,v)$ are shown in Fig. 1(a). The fixed point is located on the left branch $F_l(u,v)$.

Depending on the amplitude of an applied perturbation $f(t)$, added, e.g., in the second equation as $\dot{v} = \epsilon(u + a) + f(t)$, the system can respond in two different ways. It *either* makes small oscillations in the vicinity of the fixed point [dash-dotted line in Fig. 1(a)] *or*, for a slightly greater perturbation, it can make a large excursion from the left branch $F_l(u,v)$ to the right branch $F_r(u,v)$ and back [creating a spike, as shown by the dotted line in Fig. 1(a)]. Thus, the presence of excitability can easily be established by this simple test. It leads to the conclusion that there must exist a boundary (threshold) in the u - v phase space of the FHN system. However, this test says nothing about the structure of the threshold, which we now discuss.

Usually the presence of any threshold is related to the existence of saddle states (sets), e.g., a saddle point in the bistable Duffing oscillator ($\ddot{x} + \alpha\dot{x} + x^3 - x = 0$, where x is a variable and α is the damping coefficient) and its stable

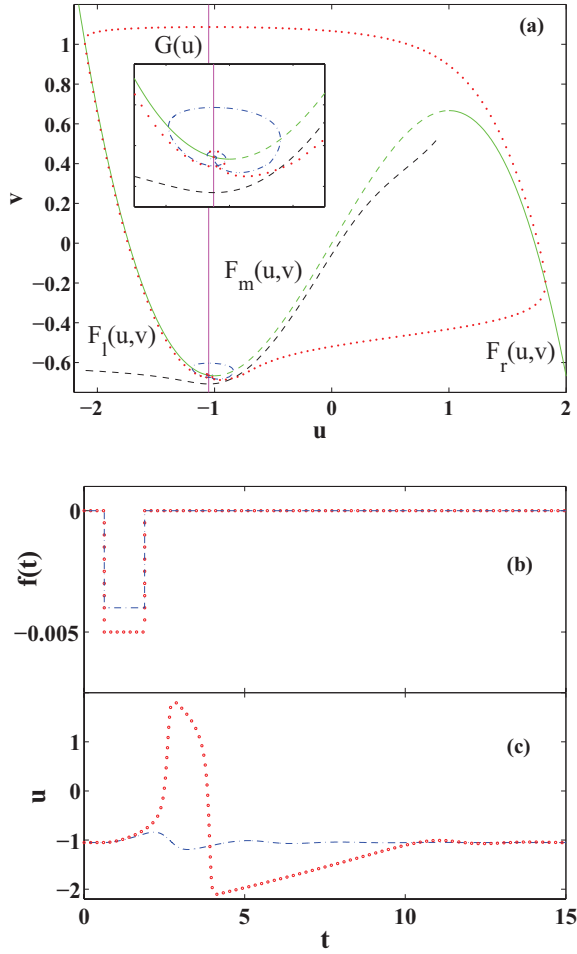


FIG. 1. (Color online) The u - v phase plane of the FHN system and the responses to the external force $f(t)$ (dimensionless units). (a) The left, middle, and right parts of the nullcline $F(u, v)$ are denoted as $F_l(u, v)$, $F_m(u, v)$, and $F_r(u, v)$, respectively. The inset shows an enlarged area of the phase plane in the close vicinity of the fixed point. The dashed (black) line corresponds to the boundary curve. The dotted and dash-dotted lines represent, respectively, the responses of the FHN system to the corresponding external forces shown in (b). Time realizations of the u coordinate are shown in (c). The parameters of the FHN system (1) are $a = 1.05$ and $\epsilon = 0.05$.

manifolds define the boundary between two stable states. In the FHN system there is no saddle state, but the threshold reveals itself when we consider the evolution of the system from different initial conditions. Depending on what these are, the trajectory goes initially to the left or right, in the direction of the left $F_l(u, v)$ or right $F_r(u, v)$ branches, and then it goes to the stable state. If the trajectory reaches the right branch $F_r(u, v)$, then a spike is generated. Thus, considering different initial conditions, we can specify a boundary between two different regions of the phase plane [the black dashed line in Fig. 1 (a)]. Note that the boundary itself corresponds to a trajectory of the system (1), i.e., if we specify initial conditions (u_0, v_0) on the boundary, then the trajectory corresponding to the solution of Eq. (1) follows the boundary.

The origin of the boundary can be understood by consideration of the singular limit $\epsilon \rightarrow 0$ [19,20] where the two branches $F_r(u, v)$ and $F_l(u, v)$ are regarded as attractors; there

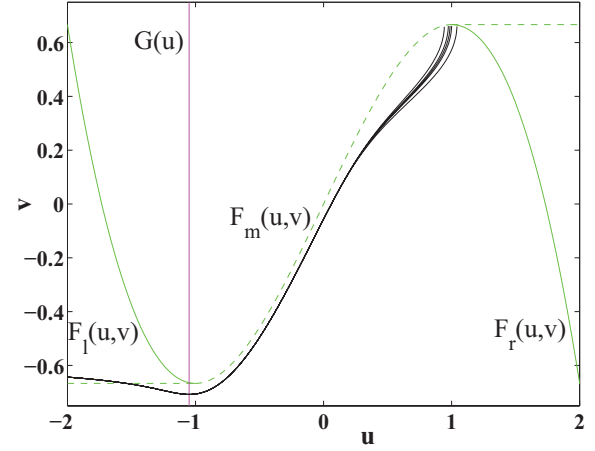


FIG. 2. (Color online) The boundary structures in the singular limit $\epsilon \rightarrow 0$ (dashed line) and for the finite value of $\epsilon = 0.05$ (solid lines) are shown in the u - v phase plane (dimensionless units). The nullcline $G(u)$ and the branches $F_l(u, v)$ and $F_r(u, v)$ are shown by solid lines and the branch $F_m(u, v)$ is shown by the dashed line. The trajectories for finite ϵ correspond to solutions of an initial value problem, i.e., they were calculated by integrating Eq. (1) directly in time for specified initial conditions (u_0, v_0) : for the curves shown, $u_0 = -3$ and v_0 has been varied. The parameters of the FHN system (1) are $a = 1.05$ and $\epsilon = 0.05$.

is a separatrix that includes the middle branch $F_m(u, v)$, and two rays $v = -2/3$, $u \in (-\infty, -1]$ and $v = 2/3$, $u \in [1, \infty)$, which start in the fold points $\partial F(u, v)/\partial u = 0$, i.e., $u = \pm 1$ and $v = \pm 2/3$ (Fig. 2). It has been shown [20] that for finite ϵ a particular line (separatrix) does not exist, and an infinite number of lines, a layer, can be specified (see the solid lines in Fig. 2), but within a distance $r \gg \epsilon$ from the fold point $(1, 2/3)$ the layer tends to one line and forms a boundary similar to the singular limit $\epsilon \rightarrow 0$, forming the boundary layer seen in Fig. 2. Therefore, we can reasonably refer to this boundary (for finite ϵ) as the “ghost separatrix” of the singular limit. Note that for finite ϵ the boundary does not coincide with the middle branch, $F_m(u, v)$.

Another way of illustrating the origin of the boundary under discussion is to consider an FHN system with three fixed points. This illustration is in line with the usual analysis of a transition to excitability via a saddle-node bifurcation [8], but the difference is that here we consider such a transition for a saddle point and it does not change the stability of the stable fixed point. Let us modify Eq. (1) in the following way:

$$\begin{aligned} \dot{u} &= u - u^3/3 - v, \\ \dot{v} &= \epsilon[u - cv + a]. \end{aligned} \quad (2)$$

Here we introduce the new parameter c , and we set $a = 1.05$, $\epsilon = 0.05$. Depending on the value of c , system (2) can have one fixed point [in which case Eq. (2) is excitable], two points at the tangent bifurcation point [21], or three points [in which case Eq. (2) becomes bistable]; the coordinates of these points are determined by intersections of the nullclines $v = u - u^3/3$ and $v = (u + a)/c$ (Fig. 3). Where there are three fixed points ($c = 3$), the manifolds of the middle (saddle) point form the boundary between the other two states. The left branch of

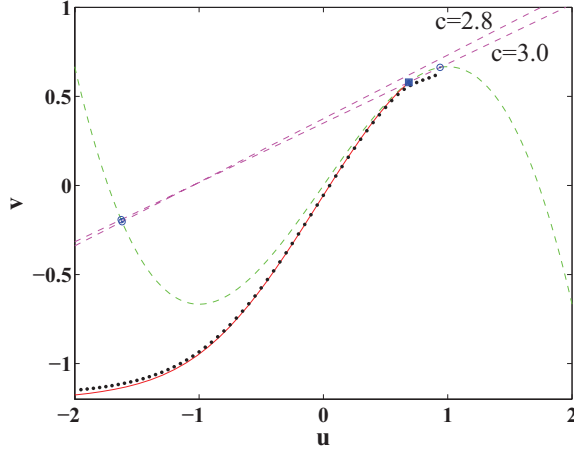


FIG. 3. (Color online) The left branch of the manifold of the middle point is shown by the solid (red) line in the u - v phase plane (dimensionless units). It was calculated from initial conditions on the eigenvector of the middle (saddle) point for $c = 3$. The boundary in the excitable regime ($c = 2.8$) is shown by the dotted (black) line. The nullclines are shown as dashed lines. The symbols \bullet and \blacksquare indicate the coordinates of fixed points, with \blacksquare indicating the saddle point. The parameters of the FHN system (2) are $a = 1.05$ and $\epsilon = 0.05$.

the manifolds of the middle point is shown by the solid line in Fig. 3. The boundary in the excitable case ($c = 2.8$) when there is no saddle point is shown by the dotted line. The behavior illustrated in Fig. 2 allows us to say that the boundary in the excitable regime is a “ghost” of the manifold of the disappeared saddle point.

This last illustration, and analysis [20] using the singular limit, demonstrate the existence of a boundary area that can be considered as being indistinguishable from a line (separatrix) far from the fold point, but there is no corresponding unstable state. It is obvious that this unusual phase-space structure requires careful analysis of the escape process.

III. LARGE FLUCTUATIONS APPROACH

A. Optimal escape path and the boundary

Noise-induced escape is usually described as a transition from a stable state to a saddle (boundary) state, and it is inferred that an escape trajectory passes via (nearby) the saddle state. Such a picture has a rigorous basis in the theory of large fluctuations [18] and it has been confirmed in many examples ranging from a simple overdamped bistable system [22] to systems with chaotic dynamics [23–26]. The saddle state is considered as the transition state and is used for calculation of the escape rate.

The fact that there is no saddle state in the excitable regime of the FHN system (1) leads us to consider a more general problem of noise-induced boundary crossing. Note that in the previous section we showed that there exists a boundary between the right $F_r(u, v)$ and left $F_l(u, v)$ branches of the nullcline $F(u, v) = 0$, and we discussed this boundary as forming a “ghost” manifold. The latter perception suggests that the boundary should possess some of the properties exhibited by the manifold of a dynamical system. One important property [18] is that the optimal escape path must not cross the manifold.

Thus, the behavior of the escape path can reveal both the boundary and its properties.

Let us consider a stochastic version of (1) in the following form:

$$\begin{aligned}\dot{u} &= u - \frac{u^3}{3} - v + \xi_u(t), \\ \dot{v} &= \epsilon [u + a] + \xi_v(t),\end{aligned}\quad (3)$$

with two additive white noise sources $\xi_u(t)$ and $\xi_v(t)$ of intensity D_u and D_v , respectively; $\langle \xi_{u,v}(t) \rangle = 0$ and $\langle \xi_u(t) \xi_v(t) \rangle = 0$. The noise $\xi_u(t)$ can be interpreted as external inputs arriving to the neuron (e.g., spikes from other neurons), whereas the noise $\xi_v(t)$ reflects internal fluctuations in the currents, e.g., through the ion channels of the neuron [27]. The noise intensities can be represented as $D_u = r_u D$ and $D_v = r_v D$ and the coefficients r_u and r_v determine which noise source is the more significant. For zero noise intensity $D = 0$ there is one stable point (u_s, v_s) , $u_s = -a$ and $v_s = -a(1 - a^2/3)$ for $a > 1$, and system (3) is in its excitable regime.

The Fokker-Plank equation describing the probability density $P(u, v, t)$ corresponding to the Langevin equation (3) takes the form [28]

$$\begin{aligned}\frac{\partial P}{\partial t} &= \frac{\partial}{\partial u} \left[- \left(u - \frac{u^3}{3} - v \right) P \right] + \frac{\partial}{\partial v} [-\epsilon(u + a)P] \\ &+ r_u D \frac{\partial^2 P}{\partial u^2} + r_v D \frac{\partial^2 P}{\partial v^2}.\end{aligned}\quad (4)$$

An equilibrium solution of (4) can be written in the WKB-like approximate form [18,29–31]

$$P(u, v) = Z(u, v) \exp[-S(u, v)/D], \quad (5)$$

where Z is a prefactor and the action S can be considered as a quasipotential of (3) [32]. Inserting the expression (5) into (4), and expanding in powers of D , allows one to obtain the equations for the action S and for the prefactor Z in the leading ($D \rightarrow 0$) and next-to-leading (finite D) orders of approximation respectively [18,29–31,33].

The leading order [18] results in the following extended system:

$$\dot{u} = \frac{\partial H}{\partial p_u}, \quad \dot{v} = \frac{\partial H}{\partial p_v}, \quad \dot{p}_u = -\frac{\partial H}{\partial u}, \quad \dot{p}_v = -\frac{\partial H}{\partial v}, \quad (6)$$

which has the Wentzel-Freidlin Hamiltonian

$$H = p_u \left(u - \frac{u^3}{3} - v \right) + p_v \epsilon [u + a] + \frac{r_u}{2} p_u^2 + \frac{r_v}{2} p_v^2 \equiv 0, \quad (7)$$

where p_u and p_v are conjugate momenta. The system determines the most probable trajectories of (3) connecting the initial $(u(t_i), v(t_i))$ and final $(u(t_f), v(t_f))$ states, i.e., trajectories driven by noise realizations having the minimal action (energy)

$$\begin{aligned}S &= \min \int_{t_i}^{t_f} dt [\xi_u^2(t) + \xi_v^2(t)] \\ &= \int_{t_i}^{t_f} dt \frac{1}{2} [r_u p_u^2 + r_v p_v^2].\end{aligned}\quad (8)$$

Because the trajectory probabilities are determined as $P \propto \exp(-S/D)$, these trajectories are the most probable paths. To determine the optimal escape path, i.e., the trajectory connecting the stable state (u_s, v_s) of (3) to the boundary (u_b, v_b) , we have to perform an additional minimization and find the trajectory with minimal action $S = S_{\min}$. Thus, we have formulated the boundary problem for (6) with two boundary conditions $[u_s(t_i), v_s(t_i), p_u(t_i) = 0, p_v(t_i) = 0]$ and $[u_b(t_f), v_b(t_f), p_u(t_f) = 0, p_v(t_f) = 0]$, with $t_i \rightarrow -\infty$ and t_f unspecified. To solve the boundary problem we follow the method described in Ref. [34]. It leads to a shooting approach, i.e., to finding a solution by consideration of different initial guesses leading to trajectories from behind the boundary to the branch $F_r(u, v)$. For the system considered (6), the shooting problem is effectively one-dimensional (there is one parameter, x , that specifies all possible initial conditions) and we are able to find the optimal escape path by considering the dependence on x of the action S . A minimum in this dependence specifies the desired path. We stress that we do not specify explicitly the second boundary condition $(u_b(t_f), v_b(t_f))$; we consider trajectories coming to the branch $F_r(u, v)$ and use the condition $[p_u(t_f) = 0, p_v(t_f) = 0]$ to verify the correctness of the calculated path. Note that in the integrator case [when the stable state of (3) is a node] it is possible to specify initial conditions explicitly on the minimal-action trajectory, which corresponds to the nonleading one-dimensional manifold of system (6).

Solutions of the boundary problem corresponding to optimal escape paths are shown in Fig. 4 for different values of the coefficients r_u and r_v and two different values of the parameter a . The optimal paths approach the boundary without crossing it and, consequently, without reaching the right branch $F_r(u, v)$. It can be seen that noises in the fast and slow variables produce quite distinctive patterns in the phase space and that these patterns depend strongly on the system and noise parameters.

The results presented in Fig. 4 demonstrate the existence of optimal paths in the FHN system within the excitable regime and thus support the conclusions drawn in Sec. II about the boundary structure.

B. Escape rate

An important measure of system stability is the escape rate, or the mean escape time T . The escape rate allows us to verify the values of the action S corresponding to optimal paths. We simulated the Langevin equations (3) numerically and estimated the time interval τ to reach the right branch $F_r(u, v)$ from initial conditions in the stable state (u_s, v_s) . By repeating the simulations we collected an ensemble of intervals τ_i and estimated the mean escape rate as $T = \frac{1}{N} \sum_{i=1}^N \tau_i$, $N = 20\,000$. The value of T can be estimated from the action S corresponding to the optimal path, because S defines a quasipotential of system (3) and the value of S on the boundary (for the optimal path) corresponds to the quasipotential barrier. It means that we may expect that $T \propto \exp(S/D)$. The calculated optimal paths yield estimates of the escape threshold S that are in excellent agreement with those derived from Eqs. (6)–(8), as shown in Fig. 5. Disagreement between the numerical results and theoretical predictions is observed only for large noise, when the mean

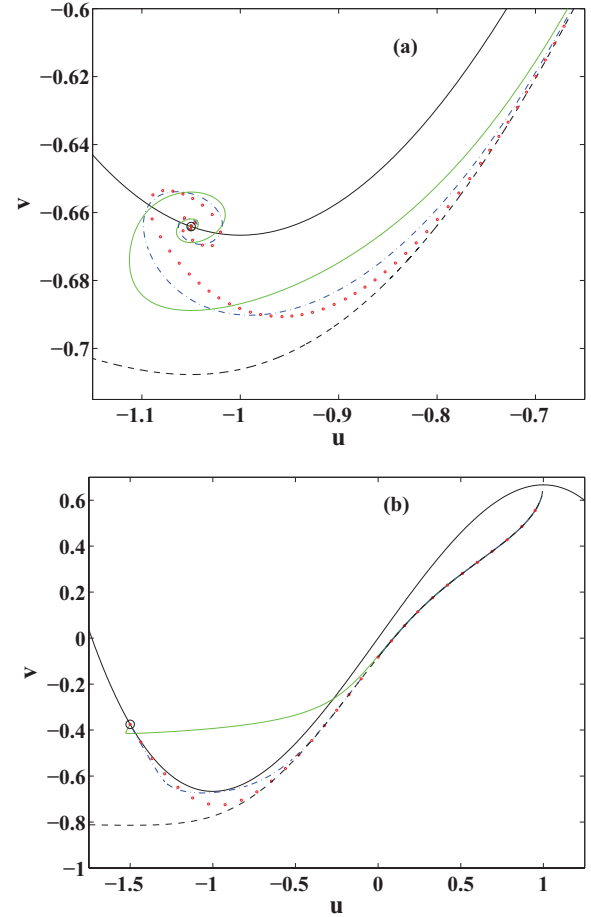


FIG. 4. (Color online) Optimal paths in the u - v phase-plane for different sets of parameters (dimensionless units): (a) $\epsilon = 0.05$, $a = 1.05$ and (b) $\epsilon = 0.05$, $a = 1.5$. The nullcline $F(u, v)$ and boundary are shown by the thin (black) solid and dashed lines, respectively. The symbol \bullet indicates the fixed point. The thick solid (green), dotted (red), and dash-dotted (blue) lines correspond to the cases $r_u = 1$ and $r_v = 0$, $r_u = 0$ and $r_v = 1$, and $r_u = 1$ and $r_v = \epsilon$.

escape time T becomes comparable to the relaxation time [35] of system (1). These results evince that, although the large fluctuation approach is based on the asymptotic limit $D \rightarrow 0$, its predictions remain valid over a wide range of small finite values of noise intensity.

C. Exit location distribution

We now compare the noise-induced escape trajectories of system (3) found by numerical simulation with the optimal paths shown in Fig. 4. The escape trajectories are shown in Fig. 6(a) together with the optimal path. It is evident that the escape trajectories approach the optimal path, but that they differ markedly from it near the boundary and cross the boundary rather than running along it. Such a situation was observed earlier (see Ref. [36] and references therein). It is known as *saddle-point avoidance* and characterized by the *exit location distribution* (ELD). The difference here, however, is that there is no saddle point, so existing theoretical approaches [31,36] for calculating the ELD are inapplicable. Note, however, that the optimal path was calculated in the

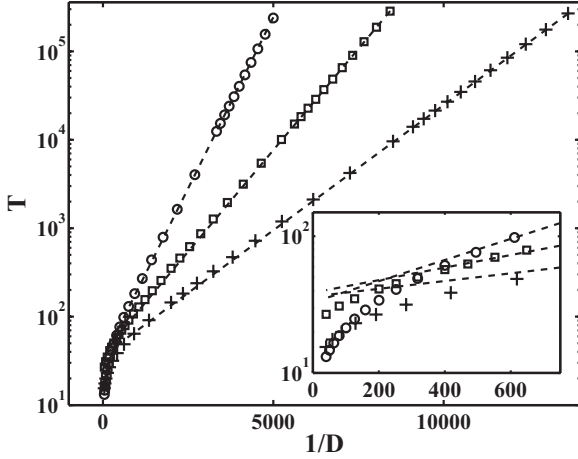


FIG. 5. The calculated mean escape times T are plotted as a function of inverse noise intensity $1/D$ for the cases (dimensionless units): \circ $r_u = 1$ and $r_v = 0$; \square $r_u = 0$ and $r_v = \epsilon$; $+$ $r_u = 1$ and $r_v = \epsilon$. The parameters are $\epsilon = 0.05$ and $a = 1.05$. The vertical axis is logarithmic. The dashed lines correspond to the approximation $T \propto \exp(\frac{S}{D})$, where S corresponds to the optimal path, i.e., the solution of the boundary value problem for Eq. (6). The inset shows the dependence $T(1/D)$ for large values of noise intensity.

limit of zero noise intensity and that the noise intensity is not included as a parameter during the calculation. This strongly suggests that the observed difference [Fig. 6(a)] may be attributable to the finiteness of the noise intensity. We can take this into account by consideration of the prefactor Z in (5) [29–31,33].

The prefactor Z can be calculated via the next-to-leading-order (finite D) approximation of the Fokker-Plank equation (4). It leads to an extension of system (6) by addition of the differential equations for the prefactor Z and the Hessian matrix \mathbf{W} , which corresponds to a matrix of the second-order derivatives of the action S with respect to system coordinates u and v . Details can be found in Refs. [31,33]. We now consider further the case where $r_u = 1$ and $r_v = 0$.

The ELD describes the distribution of points corresponding to crossing points of escape trajectories over the boundary B of some domain. The separatrix discussed in Sec. II forms this boundary and, since it is a monotonic curve (see Fig. 4, for example), the boundary, and, consequently, the ELD, can be parameterized by one variable only, i.e., $B = B(u)$. The ELD $\rho_B(u)$ of exit points on B can be determined from the solution of the stationary Fokker-Plank equation (4) with a unit source at the stable point (u_s, v_s) and an absorbing boundary condition on B [31,37,38]. The ELD is related to the probability flux via an elementary segment $dl(u)$ of $B(u)$ [31] leading to

$$\rho_B(u) = \frac{Dr_u}{N} \frac{\partial P(u,v)}{\partial u} (\mathbf{n}, \mathbf{e}_u), \quad (9)$$

where we take into account that $B(u)$ corresponds to the separatrix, which is a solution of the deterministic system (1); \mathbf{n} is the outward normal to B at (u, v) , \mathbf{e}_u is a unit vector in the u direction, and N is the normalization constant. Using the ansatz (5), the ELD is represented in terms of Z

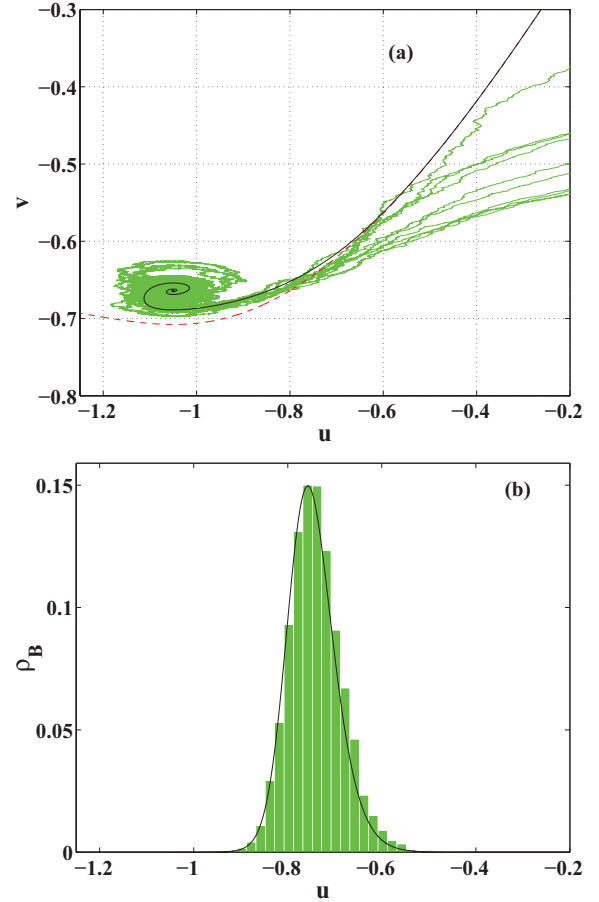


FIG. 6. (Color online) (a) Ten escape trajectories obtained by numerical simulation of (3) are shown by jagged (green) lines (dimensionless units). The optimal path is shown by the thick (black) solid line and the boundary by the dashed (red) line. (b) The escape location distribution $\rho_B(u)$ calculated via (10), and obtained by numerical simulations of (3), are shown by the solid (black) line and the (green) histogram bars, respectively. The parameters of Eq. (3) are $D = 3.25 \times 10^{-4}$, $\epsilon = 0.05$, $a = 1.05$, $r_u = 1$, and $r_v = 0$.

and S as

$$\rho_B(u) = \frac{Dr_u}{N} p_u(u,v) Z(u,v) \exp \left\{ \frac{-S(u,v)}{D} \right\} (\mathbf{n}, \mathbf{e}_u). \quad (10)$$

Values of momentum p_u , action S , and prefactor Z can be found by numerical solution of the boundary value problem with initial conditions on the stable state (u_s, v_s) and second condition on the boundary $B(u)$; the product $(\mathbf{n}, \mathbf{e}_u)$ can also be calculated numerically from the known coordinates of the boundary. The ELDs calculated from (10), and by simulation of the stochastic equation (3), are compared in Fig. 6(b). The agreement is excellent, showing that inclusion of the prefactor Z provides a satisfactory description of finite-noise effects. We stress that the technique described can also be applied straightforwardly to the case when there is a saddle point.

According to the duality between the Wentzel-Freidlin Hamiltonian formalism of large fluctuations and the Pontryagin Hamiltonian formalism of optimal control [23,25,39], the momenta p_u and p_v define the optimal fluctuational force and, equivalently, the deterministic control force that induces

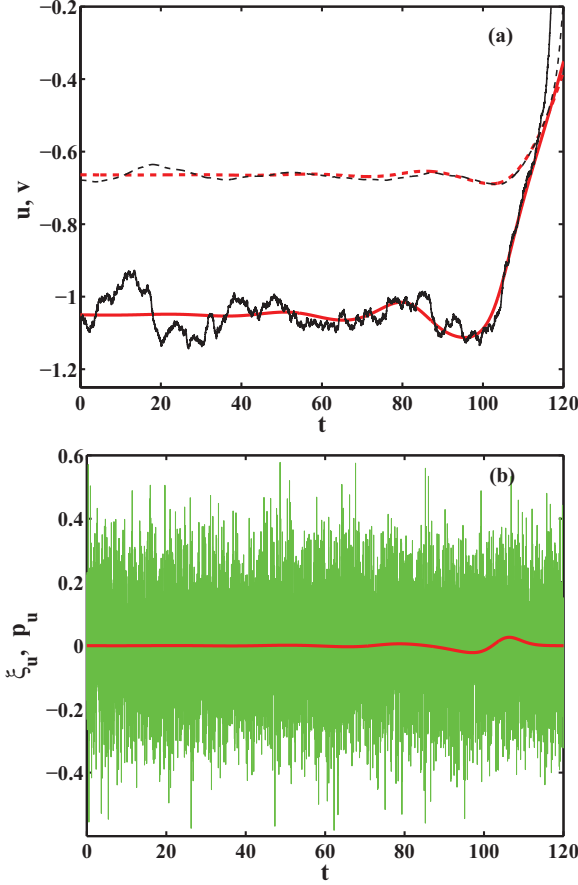


FIG. 7. (Color online) Time realizations of the optimal path and the optimal force are superimposed on numerical realizations of an escape trajectory (a) and of a noise realization (b), respectively (dimensionless units). In (a) the dashed and solid lines correspond to the coordinates u and v , respectively; the thick lines correspond to the optimal paths, whereas the thin lines show the coordinates of an escape trajectory. In (b) the thick line corresponds to the optimal force p_u , whereas the thin line shows the noise realization ξ_u . The parameters of system (3) are $\epsilon = 0.05$, $a = 1.05$, $r_u = 1$ and $r_v = 0$, $D = 3.25 \times 10^{-4}$.

the transition between states with minimal applied energy S . The above results show that the theory of large fluctuations provides a sufficient description of the fluctuational dynamics and can describe the behavior of stochastic escape trajectories. We will demonstrate below how the optimal force defined by the momenta p_u and p_v can also be used to predict the response of the system to a stimulus. First, however, we will consider the following question: Should we expect that the noise realizations leading to escape will correspond closely to the optimal fluctuational force? In Fig. 7 the coordinates of an escape trajectory and the optimal force are shown together with corresponding noise realization $\xi_u(t)$ and momentum $p_u(t)$. The latter corresponds to the optimal fluctuational force. It can be seen that the noise realization does not have any specific patterns, unlike the escape trajectories. Therefore, the answer to the question formulated above is that the optimal force is hidden within the noisy background, whereas the actual escape trajectory follows the theoretical path.

IV. LOCAL VERSUS NONLOCAL APPROACHES TO STABILITY ANALYSIS

A. Noise-induced escape in a resonator and an integrator

Currently, the main approach for analyzing the properties of a neuron (summarized in Ref. [8]) is based on (i) a purely deterministic picture and (ii) a local analysis of fixed points and the associated bifurcations. The approach that we present here corresponds to an alternative description of the neuron's properties, and it can be considered as an additional nonlinear (nonlocal) stability analysis. We stress that we consider our approach as being complementary to the existing one.

In the Izhikevich classification discussed above there is a classification property related to the character of the stability at a fixed point (node or focus), leading to an integrator or a resonator, respectively. In chapter 7 of Ref. [8] there is a summary of theoretical and experimental results to support such a classification. For example, there is a statement that one can expect frequency preference in the resonator case and an absence of frequency preference for the integrator.

Let us consider the difference in noise-activated spiking in the excitable regime of the FHN system (3) for two cases when the fixed point is either a node or a focus, i.e., an integrator or resonator. If we fix the parameter $\epsilon = 0.05$, the stability of the fixed point (u_s, v_s) is then defined by the parameter a . The eigenvalues of the fixed points are defined by the expressions $\lambda_{1,2} = 0.5[(1 - a^2) \pm \sqrt{(1 - a^2)^2 - 4\epsilon}]$. In the noise-free case system (3) undergoes a Hopf bifurcation at $a = 1$, when the eigenvalues $\lambda_{1,2}$ of the fixed point are $\lambda_{1,2} = 0 \pm i0.2236$, where $i = \sqrt{-1}$. The value of the imaginary parts of $\lambda_{1,2}$ defines the frequency $\omega_0 = 0.5[\sqrt{(1 - a^2)^2 - 4\epsilon}]$ of self-oscillation after the Hopf bifurcation or the frequency of underdamped oscillation before the bifurcation. In the range $a \in (1; 1.203)$ the eigenvalues $\lambda_{1,2}$ are complex conjugate with negative real parts, i.e., the fixed point is a focus, and the point becomes a node for $a > 1.203$, when $\lambda_{1,2}$ are real. Since the local approach [8] is based on bifurcations, its predictions include the existence of a preferred frequency $\Omega_H \leq 0.2236$ in the resonator case, and the absence of any such frequency for the integrator. In comparing these predictions with nonlocal analysis and numerical simulations of (3) we consider three cases corresponding to three different values of the parameter a as follows:

(1) $a = 1.05$. This value is very close to the Hopf bifurcation. The fixed point is a focus with eigenvalues $\lambda_{1,2} = -0.0513 \pm i0.2177$. The expected preferred frequency is $\omega_0 = 0.2177$, which is close to Ω_H . This is the resonator case.

(2) $a = 1.15$. The fixed point is a focus with eigenvalues $\lambda_{1,2} = -0.1612 \pm i0.1549$ and $\omega_0 = 0.1549$. This is the resonator case.

(3) $a = 1.25$. The fixed point is a node with eigenvalues $\lambda_1 = -0.4518$ and $\lambda_2 = -0.1107$. There is no preferred frequency according to the local approach, so $\omega_0 = 0.0$. This is the integrator case.

We recall that there is one fixed point of (3) for all these values of a . We now consider the two extreme cases where noise enters either the fast variable only ($r_u = 1$ and $r_v = 0$) or the slow variable only ($r_u = 0$ and $r_v = 1$).

First, we compare the optimal paths for the above three values of a (Fig. 8). For both types of noise the patterns

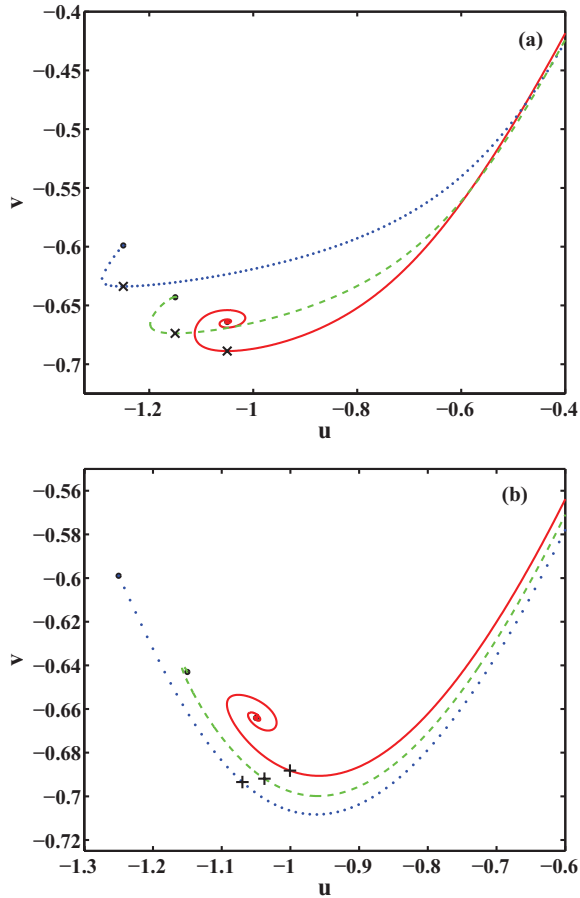


FIG. 8. (Color online) Optimal paths in the u - v phase-plane with noises in (a) the fast and (b) the slow variables for different values of the parameter a (dimensionless units): the solid (red) line corresponds to $a = 1.05$, the dashed (green) line to $a = 1.15$, and the dotted (blue) line to $a = 1.25$. The location of the fixed point is marked in each case by a small filled circle \bullet . The parameter $\epsilon = 0.05$. The crosses and pluses in (a) and (b) mark coordinates corresponding to maximal absolute values (around $t = 100$) of the optimal forces shown in Fig. 9.

of paths are similar when the system is close to the Hopf bifurcation $a = 1.05$, which is in line with the predictions of the local approach. However, for either type of noise (i.e., in the fast or slow variables) the path does not demonstrate a clear oscillatory component for the resonator (dashed green curves in Fig. 8) when $a = 1.15$. Moreover, the paths for the resonator ($a = 1.15$) and the integrator ($a = 1.25$) cases are similar, and the difference between them for noises in the fast and slow variables is much more significant than that between the paths for the resonator and the integrator. Such a picture shows that conclusions based on a local analysis are applicable in a small vicinity of the bifurcation, and both the resonator and the integrator may exhibit similar noise-induced dynamics. The reason for this behavior can be understood by consideration of the optimal forces shown in Fig. 9. For comparison, the forces are normalized to maximal absolute values. When the system is close to a Hopf bifurcation, the optimal force shows a similar oscillatory pattern regardless of the variable (fast or slow) to which the noise is added. Further from the bifurcation point $a = 1$, a difference between

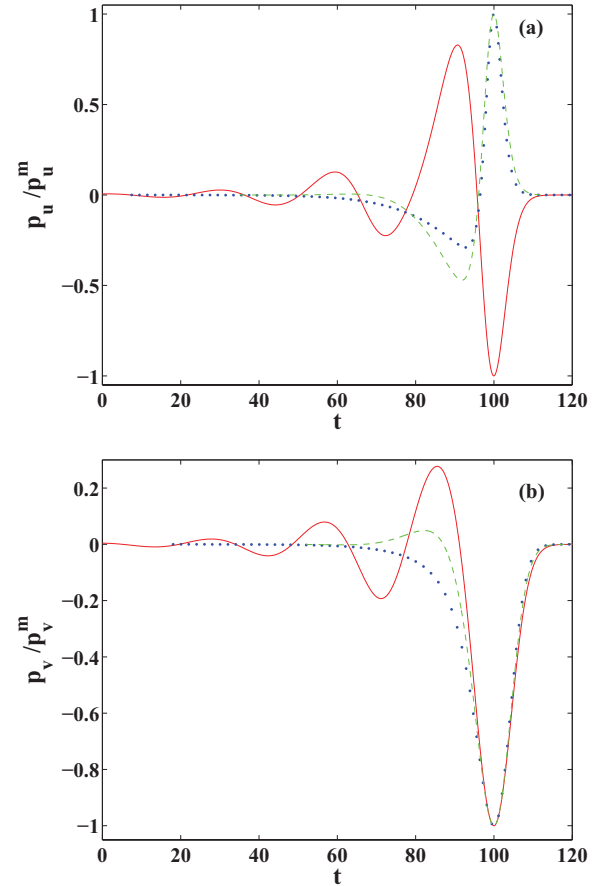


FIG. 9. (Color online) Optimal forces as functions of time t for (a) the fast, p_u , and (b) the slow, p_v , variables for different values of the parameter a (dimensionless units): The solid (red) line corresponds to $a = 1.05$; the dashed (green) line to $a = 1.15$; and the dotted (blue) line to $a = 1.25$. The forces are normalized by their maximal absolute values p^m . They correspond to solutions of the boundary value problem for system (6). The parameter $\epsilon = 0.05$.

the results of noises in the fast and slow variables becomes evident. In the case of noise in the slow variable [Fig. 9(b)] the forces differ slightly during the initial part, but they nearly coincide over the final large amplitude part when we compare the forces for different values of the parameter a . The optimal force changes significantly with increase of the parameter a in the case of noise in the fast variable, where the final large amplitude part changes sign [Fig. 9(a)].

B. Periodic driving

The description of noise-induced spikes in terms of the theory of large fluctuations (see above) allows us to reveal properties of the system and to address the question: “What kind of stimulus is needed to make a given neuron fire?” The answer lies in the optimal fluctuational forces shown in Fig. 9: Each force defines a deterministic stimulus which induces a spike by applying the minimal-energy force. These forces can also be used to describe noise-induced spikes in the presence of weak subthreshold perturbations, for example, a harmonic signal. In particular, they allow us to identify a

preferred frequency for which the spikes are most probable. The existence of such a frequency of excitation has been considered in [8] using a local bifurcational analysis to account for the experimental results [40]. Here we consider this same question but within the framework of our nonlocal approach. We therefore add a weak harmonic drive $f(t) = A \sin(\Omega t)$ to system (3) and consider the behavior of the action S that specifies the spiking rate (cf. discussion above in Sec. III).

The optimal force can be used to predict the spiking rate of the FHN system in the presence of $f(t)$ via the so-called logarithmic susceptibility [41]. The latter provides a correction, ΔS , to the action (8) obtained in the absence of driving. The modified action $S_m = S - \Delta S$ specifies the noise-induced spiking rate $T \propto \exp(S_m/D)$ in the presence of $f(t)$. The correction ΔS depends on the value of Ω and is defined [41] as

$$\begin{aligned} \Delta S &= A \sqrt{B_r^2 + B_i^2}, \\ B_i &= \frac{1}{2\pi} \int_0^{T_p} dt p(t) \cos(\Omega t), \\ B_r &= \frac{1}{2\pi} \int_0^{T_p} dt p(t) \sin(\Omega t). \end{aligned} \quad (11)$$

Here $p(t)$ is the optimal force coming from (6) and T_p is the duration of the force.

We consider two situations where the driving $f(t)$ and noise $\xi(t)$ are both added either to the first equation or to the second equation of system (3), respectively. The theoretical values of S_m are compared in Fig. 10 with those obtained from numerical simulations; the modified action S_m is normalized by the action S in the absence of harmonic driving $f(t)$, that is, for $A = 0$. Near the Hopf bifurcation $a = 1.05$, the dependence of S_m on Ω clearly shows the existence of a preferred frequency whose value is close to the prediction of the local approach $\omega_0 = 0.2177$: The value of the modified action S_m has a minimum near $\omega_0 = 0.2177$. With increase of a , the behavior of $S_m(\Omega)$ changes, showing different patterns depending on whether the noise is in the fast or slow variable. There is a nonzero preferred frequency for the case of noise in the fast variable, and it depends weakly on the parameter a . For the case of noise in the slow variable the minimal action is observed for zero frequency. Remarkably, even close to the Hopf bifurcation $a = 1.05$ there are significant differences between $S_m(\Omega)$ in Figs. 10(a) and 10(b): There is a maximum of S_m for nonzero frequency Ω separating the areas near two minima in the case of noise in slow variable. Note that the existence of a pronounced minimum (minima) in the dependencies $S_m(\Omega)$ indicates *resonant activation*, i.e., the existence of a driving frequency Ω_m that provides minimal mean activation time of the metastable state (see Refs. [42–46] and references therein for details).

In the modified action S_m , the correction ΔS is a function of Ω only and, in accordance with (11), the value of ΔS is proportional to the amplitude spectrum of the optimal force $p(t)$. Therefore, extrema in the dependence $S_m(\Omega)$ coincide with extrema in the spectrum of $p(t)$, whereas changes in the locations and number of extrema reflect changes in the shape of the optimal force $p(t)$ (see Fig. 9). We emphasize that values of frequency corresponding to extrema do not, in general, depend

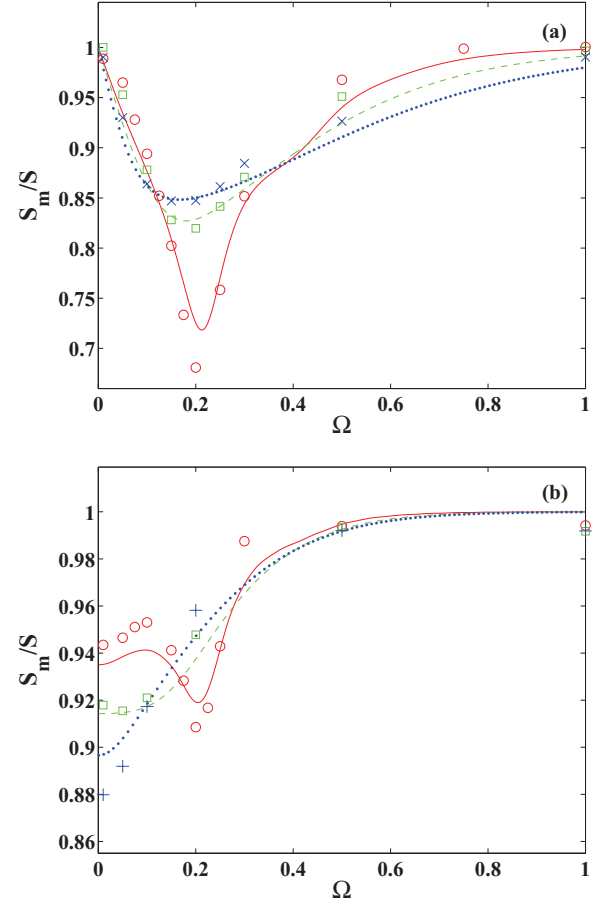


FIG. 10. (Color online) The normalized modified action S_m/S as a function of the driving frequency Ω for the combination of noise plus periodic driving in (a) the fast variable and (b) the slow variable for different values of the parameter a (dimensionless units): The solid (red) line corresponds to $a = 1.05$; the dashed (green) line to $a = 1.15$; and the dotted (blue) line to $a = 1.25$. The circles ($a = 1.05$), squares ($a = 1.15$), and crosses ($a = 1.25$) indicate the results of the corresponding numerical simulations of (3). For each value of Ω , a range of noise intensity in the simulations was selected in such a way that the mean escape times $T \in [10^4:10^5]$. The parameter $\epsilon = 0.05$.

either on the eigenvalues of the linearized system or on the type of steady state. The latter feature evidently follows from the fact that the nature of the external signal (constant value or harmonic signal at fixed frequency) is significant at all stages of escape, including the final stage of boundary crossing.

Finally, let us analyze the influence of the parameters a and ϵ on the values of the preferred frequency Ω_m , that is, on the frequency Ω of harmonic driving $f(t)$ corresponding to minimal action S_m . Using our nonlocal approach, the dependence $S_m(\Omega)$ was calculated and the corresponding Ω_m was identified for different combinations of a and ϵ . In Fig. 11(a) the resultant Ω_m (symbols) are compared with ω_0 (dashed curve) computed using the local bifurcational approach for the two cases, when both noise and $f(t)$ are acting on the fast or slow variables, respectively. The difference between these cases increases with distance from the bifurcation point $a = 1$ [Fig. 11(a)]. However, the difference also increases with a

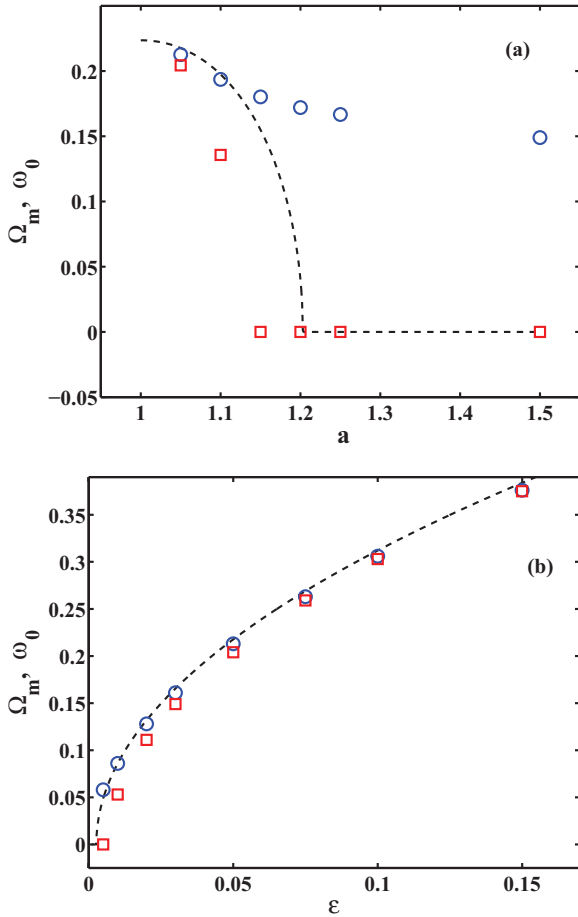


FIG. 11. (Color online) The preferred frequencies Ω_m (points) and ω_0 (dashed lines) (a) as functions of the parameter a and (b) as function of ϵ . The results corresponding to the combination of noise in the fast variable plus periodic driving, and the combination of noise in the slow variable plus periodic driving, are shown by the symbols \circ and \square , respectively. In (a) $\epsilon = 0.05$, and in (b) $a = 1.05$.

decrease of the parameter ϵ , that is, as the time-scale separation between the fast and slow variables increases [Fig. 11(b)].

The results of this section show that a deterministic classification based on local analysis of the fixed point can predict the noise-induced response and, in particular, a possible preferred frequency of the external driving, if the system is close to a bifurcation point. In the general case, however, such predictions are impossible. It then becomes necessary to consider the nonlocal (nonlinear) response based on the technique described in Secs. III and IV.

V. CONCLUSION

We have discussed the threshold structure in the excitable regime of the FHN system, when there is one fixed point only. We provided some heuristic deterministic arguments to demonstrate the presence of a threshold, and then we showed that the threshold can be revealed via analysis of the optimal fluctuational path. Further, we discussed the role of the threshold in noise-induced escape (spike generation) via analysis of the exit location distribution and a comparison

of actual escape trajectories and noise realizations with the theoretical optimal paths and forces. This approach allowed us to estimate the escape rate. An approach was developed to take account of finite noise intensity, enabling us to suggest a new technique for analytic calculation of the exit location distribution. We obtained theoretical results that are in good agreement with numerical simulations.

A comparison of the noise-induced spiking statistics with predictions based on a local analysis of the stable state, which is currently the dominant approach in neuroscience, has clearly shown that, in general, such predictions for noise-induced dynamics are not efficient. There is relatively little difference between the resonator and integrator regimes of the FHN system and, consequently, the utility of classifying them in this way is questionable for describing noise-induced dynamics, although it is clearly important for the purely deterministic case.

It was found that frequencies Ω_m corresponding to extrema of the action can differ drastically from the eigenfrequency of damped oscillations near the steady state and, furthermore, that they are weakly sensitive to the type of steady state. This peculiarity can be accounted for in terms of the nonlocal influence of the external signal over the whole escape path from the area of the metastable state's attraction. Values of the extremal frequencies coincide with locations of the extrema in the amplitude spectrum of the optimal force $p(t)$.

Our results demonstrate significant differences between the effects of noise in the fast and slow variables. They lead to different fluctuational paths in the phase space of the FHN system and they have different preferred frequencies for cases where harmonic driving is present as well as noise. The existence of such different responses can be explained on the basis of the optimal forces characterized by different patterns. The values of preferred frequency corresponding to resonant activation change significantly with variation in the system's parameters, specifying them in terms of the distance from the bifurcation point and the difference between the fast and slow time scales.

We believe that these conclusions are applicable, at least qualitatively, to other excitable systems. Note, however, that details will vary from system to system because our conclusions are based on a nonlinear analysis of the FHN, and the nonlinear response will depend significantly on the system considered.

The approach presented is based on the theory of large fluctuations which assumes the asymptotic limit of small noise but, as we have shown above, the approach is applicable far beyond the asymptotic regime for analysis of noise-induced escape. It can be extended to encompass color and other types of noise if each fluctuation term can be represented as a variable in a Langevin equation (or equations) with a white Gaussian noise source. Recently, a modified version of the Hamiltonian (7) was suggested for the case of non-Gaussian noise with finite variance (see Ref. [47] and references therein). However, if the variance is not finite, as, for example, for Levy (stable non-Gaussian) noise [48,49] then a different approach [50] must be used.

Finally, we emphasize again that the approach described in Sec. III provides an alternative way of characterizing and predicting the response of an excitable system to fluctuations

and to a mixture of periodic and stochastic stimuli. We consider it to be a further (complementary) development of the local analysis described in Ref. [8].

ACKNOWLEDGMENTS

The work was supported by EPSRC (EP/C53932X/2 and EP/G070660/1) as well as by RFBR (11-02-01418-a).

-
- [1] B. Lindner, J. Garcia-Ojalvo, A. Neiman, and L. Schimansky-Geier, *Phys. Rep.* **392**, 321 (2004).
- [2] J. White, J. Rubinstein, and A. R. Kay, *Trends in Neurosci.* **23**, 131 (2000).
- [3] J. L. A. Dubbeldam, B. Krauskopf, and D. Lenstra, *Phys. Rev. E* **60**, 6580 (1999).
- [4] M. A. Larotonda, A. Hnilo, J. M. Mendez, and A. M. Yacomotti, *Phys. Rev. A* **65**, 033812 (2002).
- [5] A. M. Yacomotti, P. Monnier, F. Raineri, B. B. Bakir, C. Seassal, R. Raj, and J. A. Levenson, *Phys. Rev. Lett.* **97**, 143904 (2006).
- [6] A. Samardak, A. Nogaret, S. Taylor, J. Austin, I. Farrer, and D. A. Ritchie, *New J. Phys.* **10**, 083010 (2008).
- [7] S. Beri, L. Mashall, L. Gelens, G. Van der Sande, G. Mezosi, M. Sorel, J. Danckaert, and G. Verschaffelt, *Phys. Lett. A* **374**, 739 (2010).
- [8] E. M. Izhikevich, *Dynamical Systems in Neuroscience: The Geometry of Excitability and Bursting*, 1st ed. (MIT Press, Cambridge, MA, 2007).
- [9] S. H. Strogatz, *Nonlinear Dynamics and Chaos: With Applications to Physics, Biology, Chemistry, and Engineering (Studies in Nonlinearity)*, 1st ed. (Perseus Books Group, Reading, Massachusetts, 1994).
- [10] A. L. Hodgkin, *J. Physiol. (London)* **107**, 165 (1948).
- [11] J. Rinzel and G. B. Ermentrout, in *Methods in Neuronal Modeling: From Synapses to Networks*, edited by C. Koch and I. Segev (MIT Press, Cambridge, MA, 1989), pp. 135–169.
- [12] V. A. Makarov, V. I. Nekorkin, and M. G. Velarde, *Phys. Rev. Lett.* **86**, 3431 (2001).
- [13] R. C. Hilborn and R. J. Erwin, *Phys. Rev. E* **72**, 031112 (2005).
- [14] B. Lindner and L. Schimansky-Geier, *Phys. Rev. E* **60**, 7270 (1999).
- [15] A. Strassberg and L. Defelice, *Neural Comput.* **5**, 843 (1993).
- [16] R. Fox, *Biophys. J.* **72**, 2068 (1997).
- [17] J. A. Armour, *Exp. Physiol.* **93**, 165 (2008).
- [18] M. I. Freidlin and A. D. Wentzel, *Random Perturbations in Dynamical Systems* (Springer, New York, 1984).
- [19] E. F. Mishchenko, Y. S. Kolesov, A. Y. Kolesov, and N. K. Rozov, *Asymptotic Methods in Singularly Perturbed Systems*, Monographs in Contemporary Mathematics (Consultants Bureau, New York, 1994).
- [20] M. Krupa and P. Szmolyan, *SIAM J. Math. Analysis* **33**, 286 (2001).
- [21] We omit a detailed description of the possible bifurcations that arise as c is varied because it is not needed for illustrative purposes. We just mention that for positive values of c there are three fixed points if $c > 2.939$ and one fixed point if $c < 2.939$. A detailed account of the possible bifurcations can be found in Ref. [8].
- [22] M. I. Dykman and M. A. Krivoglaz, *Sov. Phys. JETP* **50**, 30 (1979).
- [23] I. A. Khovanov, D. G. Luchinsky, R. Mannella, and P. V. E. McClintock, *Phys. Rev. Lett.* **85**, 2100 (2000).
- [24] V. S. Anishchenko, I. A. Khovanov, N. A. Khovanova, D. G. Luchinsky, and P. V. E. McClintock, *Fluct. Noise Lett.* **1**, L27 (2001).
- [25] D. G. Luchinsky, S. Beri, R. Mannella, P. McClintock, and I. A. Khovanov, *Intern. J. Bifurc. Chaos* **12**, 583 (2002).
- [26] I. A. Khovanov, D. G. Luchinsky, P. V. E. McClintock, and A. N. Silchenko, *Intern. J. Bifurc. Chaos* **18**, 1727 (2008).
- [27] G. Schmid, I. Goychuk, and P. Hänggi, *Fluct. Noise Lett.* **4**, L33 (2004).
- [28] H. Risken, *The Fokker-Plank Equation*, 2nd ed. (Springer, Berlin, 1993).
- [29] D. Ludwig, *SIAM Rev.* **17**, 605 (1975).
- [30] M. I. Dykman, D. G. Luchinsky, P. V. E. McClintock, and V. N. Smelyanskiy, *Phys. Rev. Lett.* **77**, 5229 (1996).
- [31] R. S. Maier and D. L. Stein, *SIAM J. Appl. Math.* **57**, 752 (1997).
- [32] R. Graham and T. Tél, *Phys. Rev. Lett.* **52**, 9 (1984).
- [33] A. V. Polovinkin, E. V. Pankratova, D. G. Luchinsky, and P. V. E. McClintock, in *Fluctuations and Noise in Biological, Biophysical, and Biomedical Systems II*, edited by D. Abbott, S. M. Bezrukov, A. Der, and A. Sanchez (SPIE, Bellingham, 2004), pp. 192–201.
- [34] S. Beri, R. Mannella, D. G. Luchinsky, A. N. Silchenko, and P. V. E. McClintock, *Phys. Rev. E* **72**, 036131 (2005).
- [35] In the linear approximation the relaxation time is equal to 20, since eigenvalues of the equalilibrium state are complex conjugate with real part $\text{Re}(\lambda) = 0.0513$.
- [36] D. G. Luchinsky, R. S. Maier, R. Mannella, P. V. E. McClintock, and D. L. Stein, *Phys. Rev. Lett.* **82**, 1806 (1999).
- [37] G. W. Gardiner, *Handbook of Stochastic Methods* (Springer-Verlag, New-York, 1982).
- [38] T. Naeh, M. Klosek, B. Matkovsky, and Z. Schuss, *SIAM J. Appl. Math.* **50**, 595 (1990).
- [39] P. Whittle, *Risk-Sensitive Optimal Control* (Wiley, Chichester, 1990).
- [40] E. M. Izhikevich, N. S. Desai, E. C. Walcott, and F. Hoppensteadt, *Trends Neurosci.* **26**, 161 (2003).
- [41] V. N. Smelyanskiy, M. I. Dykman, H. Rabitz, and B. E. Vugmeister, *Phys. Rev. Lett.* **79**, 3113 (1997).
- [42] M. H. Devoret, J. M. Martinis, D. Esteve, and J. Clarke, *Phys. Rev. Lett.* **53**, 1260 (1984).
- [43] R. Mannella and P. Grigolini, *Phys. Rev. B* **39**, 4722 (1989).
- [44] P. Bertet, I. Chiorescu, K. Semba, C. J. P. M. Harmans, and J. E. Mooij, *Phys. Rev. B* **70**, 100501 (2004).
- [45] S. Lepri and G. Giacomelli, *Phys. Rev. A* **76**, 023815 (2007).
- [46] S. S. Cherepov, B. C. Koop, Y. I. Dzhzherya, D. C. Worledge, and V. Korenivski, *Phys. Rev. Lett.* **107**, 077202 (2011).
- [47] T. Novotný, *J. Stat. Mech.* (2009) P01050.
- [48] G. Samorodnitsky and M. S. Taqqu, *Stable Non-Gaussian Random Processes: Stochastic Models with Infinite Variance* (Chapman & Hall, London, 1994).
- [49] V. V. Uchaikin and V. M. Zolotarev, *Chance and Stability, Stable Distributions and Their Applications* (VSP BV, Zeist, 1999).
- [50] P. Imkeller and I. Pavlyukevich, *Stoch. Proc. Appl.* **116**, 611 (2006).